

Numerical Analysis Study for Corrosion Near Cut Edge of Galvanized Sheet

Nobuhiro OKADA* Katsuhiko NISHIHARA
Masamitsu MATSUMOTO

Abstract

A numerical analysis model for corrosion phenomena has been developed that can calculate current densities, ion concentration and corrosion products. In this model, cathodic current density is dependent on oxygen flux and anodic current density is assumed by the Tafel equation. Current densities and ion concentration are calculated by the finite volume method. Numerical analysis results of this model verified that corrosion product distribution of Fe/Zn galvanic corrosion in NaCl solution and MgCl₂ solution obtained agreed well with that measured by the FTIR method qualitatively. Corrosion near the cut edge of the galvanized sheet was simulated and discussed. The numerical analysis result indicates that corrosion products were precipitated on the Fe surface in MgCl₂ solution and they have high corrosion resistance.

1. Introduction

The corrosion phenomena are complex wherein a variety of components and multiple reactions are intermingled, and it is difficult to elucidate the corrosion mechanism. Because in situ observation of the pH distribution and/or the ion concentration distribution during the progress of corrosion is difficult, the mechanism cannot be easily elucidated in most cases. In responding to the call for innovative improvement in measurement techniques, numerical modeling of the corrosion phenomena is gaining attention as a new method. The numerical analysis technique of structural analysis and fluid flow analysis has made great progress in recent years along with the development of computers, and several studies have also been conducted in the field of corrosion.¹⁻⁷⁾ However, these numerical analysis models are simple in nature as they only calculate for the potential and the current density distributions in solutions by defining the cathode and anode without considering the transition of pH and the precipitation reaction of corrosion products. Therefore, although the corrosion rate in an early stage can be found, they were insufficient for elucidating the corrosion mechanism as further information cannot be obtained.

We have developed a numerical analysis model that is applicable to the elucidation of the corrosion mechanism by taking into consideration the potential and current density distributions, ion and mo-

lecular migration and the equilibrium reaction and precipitation reaction of corrosion products in a solution.^{8,9)} Hereunder, we present the outline of the numerical analysis model, and report the results of the application thereof to the corrosion phenomena of galvanized steel sheets, and the study on the early stage corrosion mechanism⁹⁾.

2. Mathematical Model

The flow chart of the calculation of the numerical model is shown in **Fig. 1**. The geometry data, components and the polarization characteristics of the electrolyte solution are input as the computation condition. The specific conductance σ of the solution is calculated by Expression (1) using the electrolytic component concentrations, where F : Faraday constant, N : total number of ion species i , z_i , u_i , c_i : valence, mobility and concentration of ion species i .

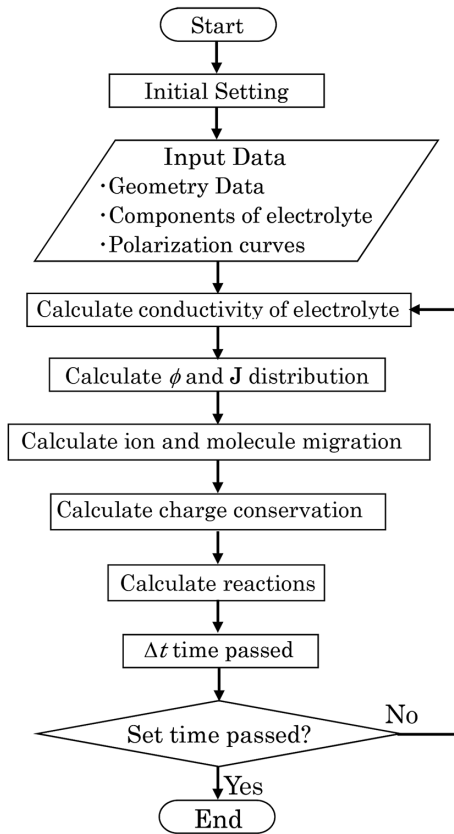
$$\sigma = F^2 \sum_{i=1}^N z_i^2 u_i c_i \quad (1)$$

Next, the potential and current density distributions are calculated. The subject parameters are the potential ϕ and the current density vector \mathbf{J} , and calculated by Laplace's equation of Equation (2).

$$0 = \nabla \cdot \mathbf{J} = \nabla \cdot (-\sigma \nabla \phi) \quad (2)$$

As the boundary conditions of Equation (2), the polarization characteristics of the anodic current density J_a and the cathodic current density J_c on metal surfaces are required. **Figure 2** shows the sche-

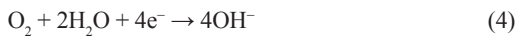
* Senior Researcher, Doctor of Engineering, Mathematical Science & Technology Research Lab., Advanced Technology Research Laboratories 20-1 Shintomi, Futtsu City, Chiba Pref. 293-8511


 Fig. 1 Flowchart of calculation⁹⁾

matic representation of polarization curves. The anodic current density is approximated by the Tafel equation of Equation (3), where corrosion potential: ϕ_0 , equilibrium current density J_{a0} and Tafel constant: α . Tafel constant α is determined as: $\alpha_{\text{zinc}} = 1.2$, $\alpha_{\text{steel}} = 0.38$, $J_{a0, \text{zinc}} = 0.25$ (A/m²) and $J_{a0, \text{steel}} = 0.18$ (A/m²). These are the values obtained by fitting the calculation result of the polarization model to the measurement result of the polarization in the NaCl 5%wt solution. Tafel constant α denotes the gradient of the anodic current density with respect to the potential, and R , T and n denote respectively gas constant, temperature, and valence without symbol.

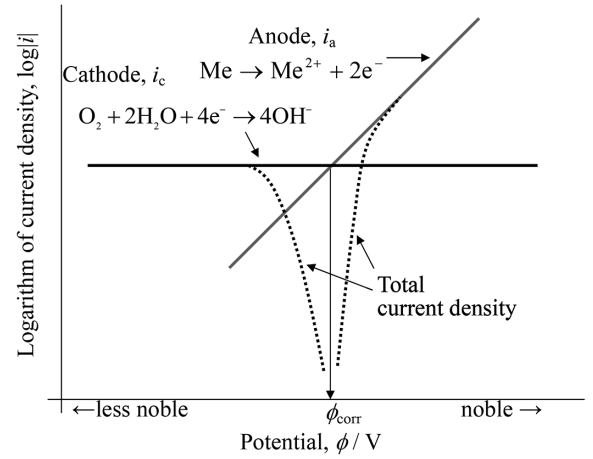
$$J_a = J_{a0} \exp \left\{ (\phi - \phi_0) \frac{\alpha n F}{RT} \right\} \quad (3)$$

The cathodic current density is not dependent on the potential above $-1.2\text{V}/\text{Ag-AgCl}$ where the hydrogen reduction reaction is negligible and the oxygen reduction reaction shown by Expression (4) is dominant. Accordingly, the cathodic current density is determined by the flux of oxygen that reaches a unit surface area of the metal in a unit time, and expressed by Expression (5), where N_{O_2} is the flux of oxygen that reaches a unit surface area of the metal in a unit time (mol/m²s).



$$\mathbf{J}_c = 4F N_{\text{O}_2} \quad (5)$$

The oxygen concentration in the solution c_{O_2} is calculated by the diffusion equation of Equation (6), where D is the diffusion coefficient. In a stationary state, the oxygen concentration is assumed to be saturated at the solution surface contacting the atmosphere. However, when the concentration is dependent on the solution rate, the solution rate is taken into consideration in the calculation.¹⁰⁾


 Fig. 2 Schematic representation of polarization curves⁹⁾

$$\frac{\partial c_{\text{O}_2}}{\partial t} = \nabla \cdot (D \nabla c_{\text{O}_2}) \quad t: \text{time} \quad (6)$$

From the obtained current density distribution, the amount of timewise ion concentration change is calculated by Expression (5). The first term of the right side of Equation (7) denotes the migration of ions by current and the second term denotes the migration by diffusion, where t_i is the transport number of the ion species i and is calculated from Expression (8). R_i of the third term is the rate of generation or the rate of consumption due to reactions.

$$\frac{\partial c_i}{\partial t} = -\nabla \cdot \left(\frac{t_i}{F z_i} \mathbf{J} \right) + \nabla \cdot (D_i \nabla c_i) + R_i \quad (7)$$

$$t_i = \frac{z_i^2 u_i c_i}{\sum_{j=1}^N z_j^2 u_j c_j} \quad (8)$$

The ion concentration distribution after a minute obtained from Expression (7) is not ensured to satisfy the electrical neutrality condition. Therefore, the ion concentration distribution needs to be corrected to satisfy the electroneutrality. When the electroneutrality is not satisfied, the potential is produced by the local charge density difference. The potential denoted as Φ is expressed by Poisson's Equation of (9), where ε is the conductivity.

$$\nabla^2 \Phi = -\frac{F}{\varepsilon} \sum_{i=1}^N z_i c_i \quad (9)$$

The coefficient of the right side term of Equation (9) is a very large value, which means that when a potential difference takes place in an actual solution, ions migrate immediately to counteract the potential difference. In implementing numerical analysis, this coefficient of large value destabilizes the computation, therefore, the standardized potential P as shown by Expression (10) which is equivalent to the potential Φ is used for computation.

$$\nabla^2 P = -\sum_{i=1}^N z_i c_i \quad (10)$$

To satisfy the electroneutrality, ions migrate along the gradient of potential P so that the charge density difference between the anion and cation becomes zero. The migration amount of the ions is termed as corrected ion flux η_i , and defined as Expression (11), assuming that the migration amount of respective ion species is proportional to its transport number.

$$\eta_i = -\frac{t_i}{z_i} \nabla P \quad (11)$$

From Expression (11), the corrected ion concentration c_i' becomes $c_i' = c_i - \nabla \cdot \eta_i$. In order for the corrected ion concentration to satisfy

the electroneutrality, the charge density should become zero, and Expression (12) is formed.

$$\sum_{i=1}^N z_i (c_i - \nabla \cdot \boldsymbol{\eta}_i) = 0 \quad (12)$$

By inserting Expression (10) into Expression (12), Expression (13) is formed.

$$\sum_{i=1}^N z_i (c_i - \nabla \cdot (-\frac{t_i}{z_i} \nabla P)) = \sum_{i=1}^N z_i c_i + \sum_{i=1}^N (\nabla(t_i \nabla P)) = 0 \quad (13)$$

As the total sum of the transport number in Expression (8) is 1 (one), Expression (13) becomes Expression (10). Expression (10) is a general Poisson's equation, and by solving the equation, the ion concentration is corrected, and the electroneutrality is possibly satisfied.

The computation was implemented based on the equilibrium theory, assuming that the reaction rate in the solution is sufficiently high and the rate is fusion-rate-determined. Specifically, although each cell is in a state of nonequilibrium immediately after the completion of the computation of ion migration, the computation is continued so that each reaction satisfies the solubility product or the equilibrium constant instantaneously. Many of the reaction rates of chemical reactions in corrosion are unknown, and it is difficult for analysis other than the computation method to find them; however, if there is a big difference among reaction rates, modelling of a certain type is required.

The simultaneous calculation method of the three reactions shown in expressions (14) to (16) is explained as an example of the reaction calculations.



Where K is the equilibrium constant and the solubility product of each reaction.

The concentrations of molecules and ions in the nonequilibrium state immediately after the migration of ions are assumed as $[\text{H}_2\text{O}]$, $[\text{H}^+]$, and the concentrations after reaching the state of equilibrium are assumed as $[\text{H}_2\text{O}]_e$, $[\text{H}^+]_e$. Further, assuming the amounts of the changes of concentrations of H_2O , H_2CO_3 and ZnCO_3 in each reaction as x_1 , x_2 and x_3 , the concentrations after reaching the state of equilibrium are expressed by Expression (17).

$$\left. \begin{aligned} [\text{H}_2\text{O}]_e &= [\text{H}_2\text{O}] - x_1 \\ [\text{H}_2\text{CO}_3]_e &= [\text{H}_2\text{CO}_3] - x_2 \\ [\text{ZnCO}_3]_e &= [\text{ZnCO}_3] - x_3 \end{aligned} \right\} \quad (17)$$

Similarly, the concentrations of other components after reaching the state of equilibrium are expressed as Expression (18) by using x_1 , x_2 and x_3 .

$$\left. \begin{aligned} [\text{H}^+]_e &= [\text{H}^+] + x_1 + 2x_2 \\ [\text{OH}^-]_e &= [\text{OH}^-] + x_1 \\ [\text{CO}_3^{2-}]_e &= [\text{CO}_3^{2-}] + x_2 + x_3 \\ [\text{Zn}^{2+}]_e &= [\text{Zn}^{2+}] + x_3 \end{aligned} \right\} \quad (18)$$

From Expressions (17) and (18), the function f that expresses the difference between the concentration product and the equilibrium constant is defined as Expression (19). If the respective reaction is in the state of equilibrium, f_1 - f_3 become 0 (zero). Therefore, by solving Expression (19), amounts of change are obtained and the concentrations after reaching the state of equilibrium are determined.

$$\left. \begin{aligned} f_1 &= [\text{H}^+][\text{OH}^-] - K_1 = ([\text{H}^+] + x_1 + 2x_2)([\text{OH}^-] + x_1) - K_1 \\ f_2 &= [\text{H}^+]^2[\text{CO}_3^{2-}] - K_2[\text{H}_2\text{CO}_3] \\ &= ([\text{H}^+] + x_1 + 2x_2)^2([\text{CO}_3^{2-}] + x_2 + x_3) - K_2([\text{H}_2\text{CO}_3] - x_2) \\ f_3 &= [\text{Zn}^{2+}][\text{CO}_3^{2-}] - K_3 = ([\text{Zn}^{2+}] + x_3)([\text{CO}_3^{2-}] + x_2 + x_3) - K_3 \end{aligned} \right\} \quad (19)$$

Where, because Expression (19) includes terms of second order, the calculation is implemented using the Newton method¹¹⁾. In the Newton method, the initial values of parameters x_1 , x_2 and x_3 are set suitably, and by adding the correction of Δx_i at each repetition computation stage, the ultimate solution of $f=0$ is obtained.

Specifically, the value of the next step of $n+1$ is approximated by the first order of Taylor's series, using the value of the current step of n . Assuming that $f=0$ is obtained in the next step, Expression (20) is formed. Expression (20) is solved with respect to the parameters of Δx_1 - Δx_3 and the amount of change is corrected based on Expression (21). This computation is repeated until $f=0$ is considered to be reached.

$$\left. \begin{aligned} f_1^{n+1} &= f_1^n + \frac{\partial f_1^n}{\partial x_1} \Delta x_1 + \frac{\partial f_1^n}{\partial x_2} \Delta x_2 = 0 \\ f_2^{n+1} &= f_2^n + \frac{\partial f_2^n}{\partial x_1} \Delta x_1 + \frac{\partial f_2^n}{\partial x_2} \Delta x_2 + \frac{\partial f_2^n}{\partial x_3} \Delta x_3 = 0 \\ f_3^{n+1} &= f_3^n + \frac{\partial f_3^n}{\partial x_2} \Delta x_2 + \frac{\partial f_3^n}{\partial x_3} \Delta x_3 = 0 \end{aligned} \right\} \quad (20)$$

$$\left. \begin{aligned} x_1^{n+1} &= x_1^n + \Delta x_1 \\ x_2^{n+1} &= x_2^n + \Delta x_2 \\ x_3^{n+1} &= x_3^n + \Delta x_3 \end{aligned} \right\} \quad (21)$$

Because these reaction calculations have to be repeated at every time step in all cells, the more reactions there are to be considered, the longer the computation time becomes.

Presently, the molecular ion species considered in the corrosion analysis model are shown in **Table 1**^{12,13)} and their reactions are shown in **Table 2**¹⁴⁻¹⁷⁾ The ion mobility μ is calculated from the ultimate mol specific conductance λ , using Expression (14).¹²⁾

$$\lambda_i = |z_i| F^2 \mu_i \quad (22)$$

Additionally, the oxygen solubility of the solution considers the salting-out effect. The oxygen solubility is expressed by the approximation (23), where T : absolute temperature of the solution, c : concentration of the solute and k_s : salting-out coefficient. In the case that pluralities of the ion species exist, $k_s \cdot c$ of Expression (23) is calculated from Expression (24),¹⁸⁾ where H_i is the salting-out parameter H of ion species i shown in Table 1.

Table 1 Values of equivalent conductance, diffusion coefficients and salting-out parameters⁹⁾

Species	$\lambda \times 10^4$ ($\text{Sm}^2\text{mol}^{-1}$)	$D \times 10^9$ (m^2s^{-1})	H	Species	$\lambda \times 10^4$ ($\text{Sm}^2\text{mol}^{-1}$)	$D \times 10^9$ (m^2s^{-1})	H
OH^-	197.6	5.26	0.340	Ca^{2+}	59.50	0.7920	-0.015
Cl^-	76.34	2.032	0.257	Fe^{2+}	54.0	0.72	-
CO_3^{2-}	41.05	1.105	-	Zn^{2+}	53.0	0.71	-0.024
SO_4^{2-}	80.0	1.065	0.163	Mg^{2+}	53.06	0.706	-0.025
H^+	349.8	9.312	-0.200	Al^{3+}	61.0	0.5414	-0.018
K^+	73.52	1.957	-0.013	H_2CO_3	-	1.9	-
Na^+	50.11	1.334	0.0	O_2	-	1.9	-

Table 2 List of reactions⁹⁾

No.	Reactions	Log K
1	$H_2O \leftrightarrow H^+ + OH^-$	-14.0
2	$H_2CO_3 \leftrightarrow 2H^+ + CO_3^{2-}$	-16.6
3	$Zn^{2+} + CO_3^{2-} \leftrightarrow ZnCO_3 \downarrow$	-10.15
4	$Zn^{2+} + 6/5OH^- + 2/5CO_3^{2-} \leftrightarrow 1/5 \{3Zn(OH)_2/2ZnCO_3\} \downarrow$	-14.2
5	$Zn^{2+} + 2/5Cl^- + 8/5OH^- \leftrightarrow 1/5 \{ZnCl_2/4Zn(OH)_2\} \downarrow$	-14.95
6	$Zn^{2+} + 2/7Cl^- + 12/7OH^- \leftrightarrow 1/7 \{ZnCl_2/6Zn(OH)_2\} \downarrow$	-15.75
7	$Zn^{2+} + 2OH^- \leftrightarrow Zn(OH)_2 \downarrow$	-16.72
8	$Fe^{2+} + 2OH^- \leftrightarrow Fe(OH)_2 \downarrow$	-15.0
9	$Mg^{2+} + 2OH^- \leftrightarrow Mg(OH)_2 \downarrow$	-10.92
10	$Mg^{2+} + CO_3^{2-} \leftrightarrow MgCO_3 \downarrow$	-4.59
11	$Ca^{2+} + CO_3^{2-} \leftrightarrow CaCO_3 \downarrow$	-8.05
12	$Al^{3+} + 3OH^- \leftrightarrow Al(OH)_3 \downarrow$	-31.7
13	$Ca^{2+} + 2OH^- \leftrightarrow Ca(OH)_2 \downarrow$	-5.10

$$C_{O_2}(T, c) = 8.18 \times 10^{-2} \exp(-1.92 \times 10^{-2} T) \cdot 10^{-k_s \cdot c} \quad (23)$$

$$k_s \cdot c = -\frac{1}{2} \sum_{i=1}^n H_{T_i}^2 c_i \quad (24)$$

By implementing the above computation expansively timewise, the nonstationary corrosion phenomena can be calculated.

3. Result of Numerical Analysis

3.1 Comparison with experiment

Pertaining to the geometries shown in Fig. 3 that represent a simple flat sheet and a simulated cut edge of a galvanized steel sheet, the results of the numerical model analysis and experiment regarding Fe and Zn were compared.⁸⁾

The results of the numerical analysis and the experiment are shown in Fig. 4 and Fig. 5. Figure 4 shows the case of NaCl 500ppm solution, and Fig. 5 shows the case of MgCl₂ 500ppm solution. (a) shows the photomicrograph of the specimens dried after immersion in solutions for 1600 seconds, (b) shows the distributions of Fe and Zn obtained by elemental analysis, and (c) shows the analysis results obtained by the Fourier transformation IR (FTIR) method and the numerical analysis for comparison.

As for the case of NaCl solution shown in Fig. 4, the photomicrograph of the test specimen after corrosion shown in (a) shows that the corrosion products are generated abundantly in the neighborhood of the Fe/Zn interface and on the Zn surface apart from Fe. In the elemental analysis result shown in (b), as the amount of the corrosion products is small, only the substrates of Fe and Zn of the test specimens were detected. In (c) that shows the distributions of the intensities of OH radicals obtained by the FTIR method and the calculation result of Zn(OH)₂ obtained by the numerical analysis, the highest peak appears on the Fe side of the Fe/Zn interface, and the intensity drops once and rises afterwards on the Zn side apart from Fe. These distribution trends are identical.

As for the MgCl₂ solution shown in Fig. 5, the photomicrograph of the test specimen in (a) shows that the corrosion products are generated on the entire surface of the Fe side apart from the interface by about 3 mm, and in the neighborhood within 5 mm from the interface on the Zn side. From the elemental analysis result shown in (b), it was confirmed that the corrosion products on the Fe surface contain Mg. From the numerical analysis result, the corrosion products were presumed to be Mg(OH)₂, the distribution of which agreed well with that of the result obtained by the FTIR method.

Thus, although quantitative evaluation is difficult, it was con-

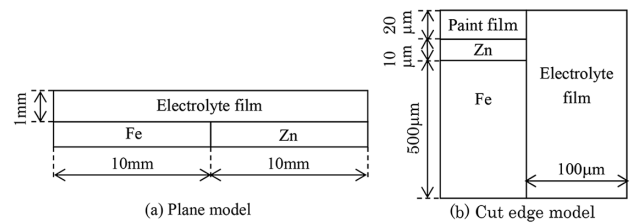


Fig. 3 Schematic diagram of numerical analysis geometry⁹⁾

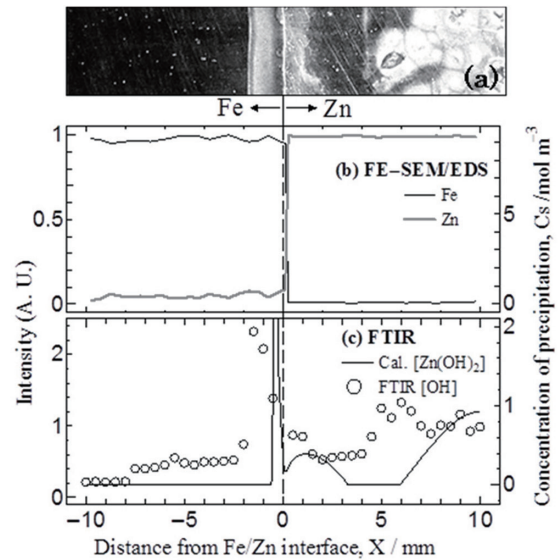


Fig. 4 (a) Photograph of a specimen, (b) Distribution of FE-SEM/EDS intensity and (c) Corrosion products obtained by numerical analysis and by FTIR after immersion in 500ppm NaCl solution for 1600 s⁹⁾

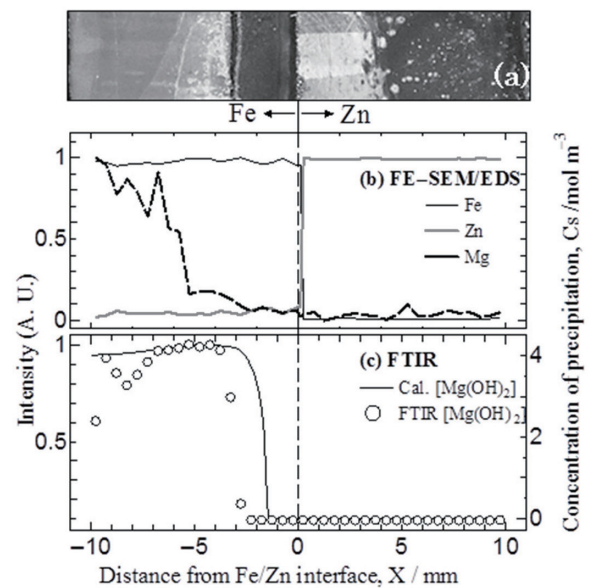


Fig. 5 (a) Photograph of a specimen, (b) Distribution of FE-SEM/EDS intensity and (c) Corrosion products obtained by numerical analysis and by FTIR after immersion in 500ppm MgCl₂ solution for 1600 s⁹⁾

firm that the trend of the distribution of the corrosion products obtained by the numerical analysis agrees well with that of the experiment result.

3.2 Study on cut edge surface corrosion

The cathodic protection on the cut edge surface of a galvanized steel sheet is insufficient; therefore, corrosion on this part often becomes problematic. For the study thereon, a numerical analysis was implemented using the computation model geometry shown in Fig. 3(b). The following salt solutions were used for the study, and results were compared; three low concentration salt solutions of NaCl 500ppm, MgCl₂ 500ppm and artificial sea water diluted to 1/100 (hereinafter referred to as ASW 1/100), and three high concentration salt solutions of NaCl 50000ppm, MgCl₂ 50000ppm and artificial sea water (hereinafter referred to as ASW 1.0). The Cl⁻ of ASW 1.0 is about 30000ppm in terms of NaCl concentration. The solution film thickness was set at 100μm, and the subsurface concentrations of oxygen and carbon dioxide of the solution were assumed as saturated.

As major components of the artificial sea water, Na⁺, Mg²⁺, Ca²⁺,

K⁺, Cl⁻ and SO₄²⁻ were considered. Although the concentration of each component conforms to ISO 11130, a small adjustment was made for the ASW to satisfy the electrical neutrality condition. As a result, the following values of concentrations were used: [Na⁺]=0.475, [Cl⁻]=0.560, [Mg²⁺]=0.055, [Ca²⁺]=0.010, [SO₄²⁻]=0.027 and [K⁺]=0.009.

Figure 6 shows the result of the numerical analysis for the low salt concentration solutions, and shows the distributions of pH, ions and the corrosion products after the immersion for 200s. Figure 6 shows that Zn²⁺ elutes from the galvanized coating part and Cl⁻ is enriched in the neighborhood thereof under any types of solution. As the Fe surface is protected by galvanic corrosion, Fe²⁺ does not elute out. As the cathodic reaction by oxygen reduction progresses on the Fe surface, OH⁻ increases and the pH increases to almost 12. The OH⁻ so increased is consumed by the precipitation reaction with Zn²⁺ in the neighborhood of the galvanized coating part, and pH in the area decreases.

In the case of NaCl solution, Zn²⁺ moves toward the Fe side by the sacrificial corrosion current, and OH⁻ moves toward the galva-

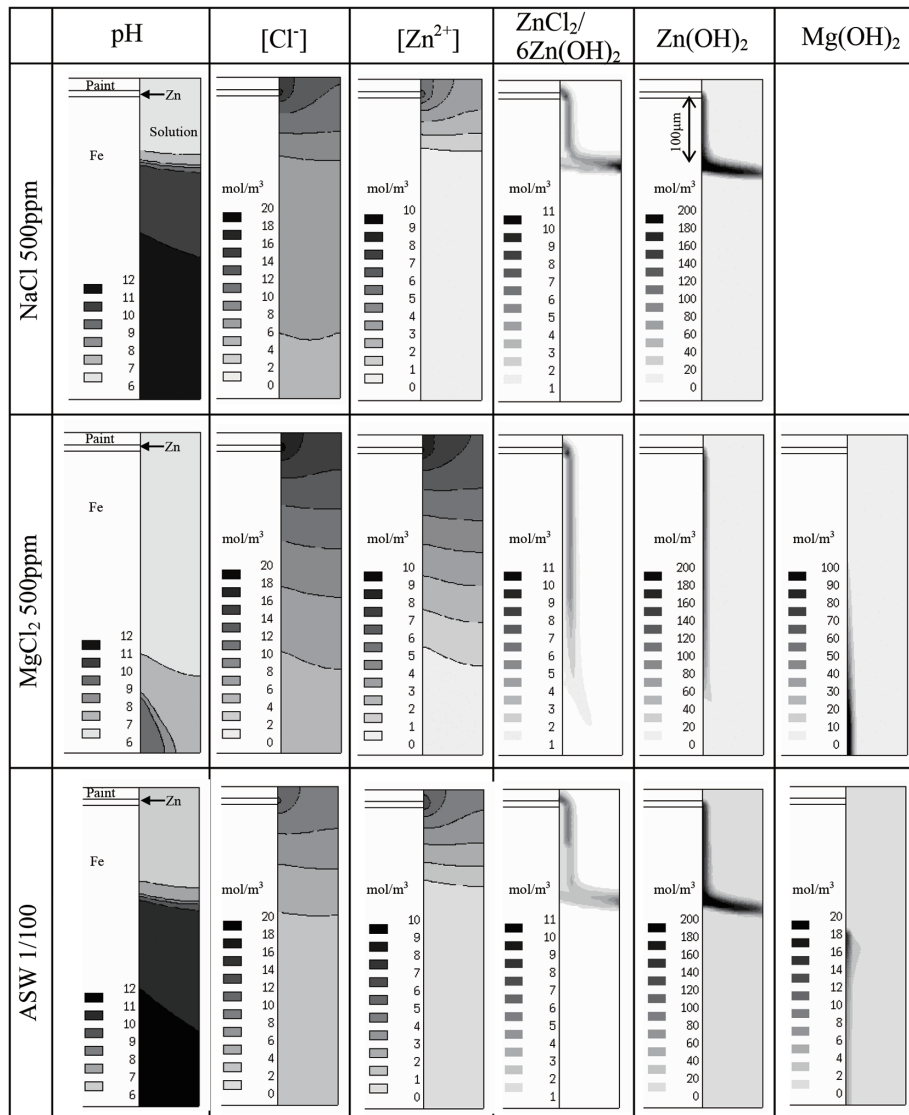


Fig. 6 Results of numerical analysis at shear cut edge of galvanized steel sheet under low salt concentration solution⁹⁾

nized coating part. The Zn^{2+} and OH^- encounter at the position about $100\mu m$ apart from the galvanized coating part, where they exceed the solubility product and are precipitated.

In the case of $MgCl_2$ solution, the corrosion products of the Zn system exist on the Fe surface near the galvanized coating part, and $Mg(OH)_2$ is generated apart from it. By examining the chronological change of the corrosion products, the following phenomenon was confirmed. $Mg(OH)_2$ is generated on the entire Fe surface right after immersion, and as pH in the neighborhood of the galvanized coating part decreases, $Mg(OH)_2$ near the galvanized coating part re-resolves, and corrosion products of the Zn system are generated instead. Namely, this finding suggests that, in the case of $MgCl_2$ solution, corrosion products remain on the Fe surface permanently. From a past experiment result, as compared with NaCl solution, higher corrosion resistance is known in $MgCl_2$ solution,¹⁹⁾ and the corrosion resistance is considered to be improved by the barrier effect of the corrosion products on the Fe surface. In the case of artificial sea water, the corrosion products distribution stays somewhere

between those in NaCl solution and $MgCl_2$ solution, and the corrosion products of the Zn system are generated on the Fe surface for about $150\mu m$ from the galvanized coating part, and are not generated farther. However, as the solution contains Mg^{2+} , $Mg(OH)_2$ is generated on the Fe surface.

Figure 7 shows the results of the numerical analysis for the case of high salt concentration solutions. In the case that the Cl^- concentration is high, as basic zinc chloride constitutes the corrosion products mainly, $Zn(OH)_2$ that precipitated in the low salt concentration solutions is not generated, however, the trend in the corrosion products distribution does not differ significantly from the one in the case of low salt concentration solutions. Presumably, the difference is that the basic zinc chloride grows more thickly in the thickness direction. This is because the basic zinc chloride exceeds its solubility product with ease even at a position away from the metal surface due to high Cl^- concentration in the solution.

In the case of NaCl 50000ppm solution in Fig. 7, similarly to the case of the low salt concentration solution, corrosion products

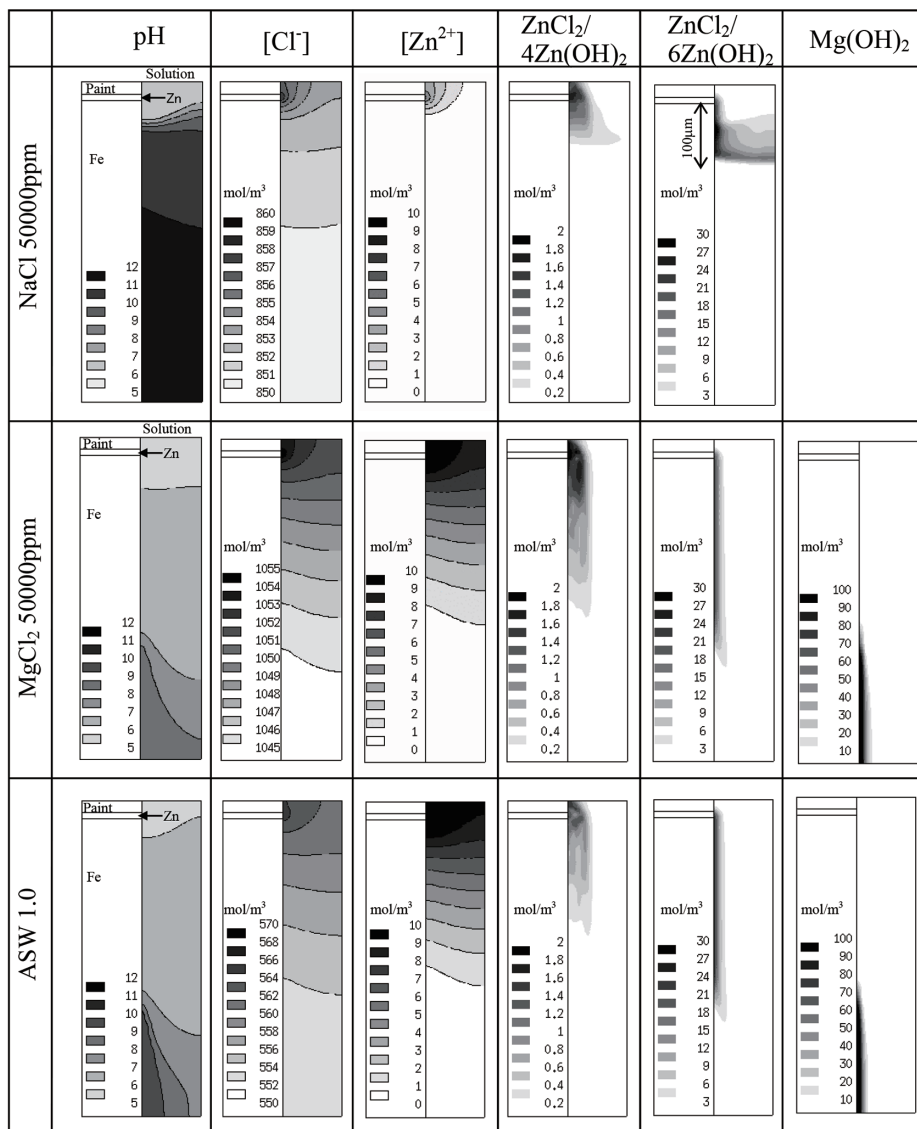


Fig. 7 Results of numerical analysis at shear cut edge of galvanized steel sheet under high salt concentration solution⁹⁾

are generated on the Fe surface to about only 100 μm from the galvanized coating part. In the case of the film thickness of 100 μm , even under the low salt concentration of 500ppm, the entire edge was protected by the cathodic protection. Therefore, the effect of the salt concentration is considered to be negligibly influential. In either case of MgCl_2 solution or artificial sea water, similarly to the case of the low salt concentration solution, $\text{Mg}(\text{OH})_2$ is generated, and there is no significant change in the corrosion product distribution.

When Mg^{2+} is contained in a solution regardless of the salt concentration difference, $\text{Mg}(\text{OH})_2$ is generated on the Fe surface and the corrosion resistance is considered to be improved thanks to the barrier effect. Additionally, as the solubility product of $\text{Mg}(\text{OH})_2$ is higher than that of $\text{Fe}(\text{OH})_2$ as shown in Table 2, in the case that Fe^{2+} exists, $\text{Fe}(\text{OH})_2$ is generated ahead, and $\text{Mg}(\text{OH})_2$ is not generated. $\text{Mg}(\text{OH})_2$ is generated only when the Fe surface is protected by the galvanic corrosion.

3.3 Study on corrosion beneath coating film near cut edge surface

As corrosion on the cut edge surface progresses, the solution intrudes into the gap of the galvanized coating that has disappeared, and corrosion beneath the coating film progresses. This model considers the change in the geometry corresponding to the corrosion

rate.²⁰⁾ However, as the corrosion progress rate and the ion migration rate, and the time to be considered therefor are far apart from each other, an extremely long computation time is required to calculate these two progresses simultaneously. Accordingly, simulating the galvanized coating retrograding due to corrosion, a numerical analysis was implemented using the geometry of the calculation model of Fig. 3 (b), with modification that the galvanized coating had retrograded by 500 μm .

Figure 8 and Fig. 9 show the results of the numerical analyses for NaCl 500ppm solution and MgCl_2 500ppm solution after the immersion for 200s.

In the case of NaCl 500ppm solution shown in Fig. 8(a), the pH of the solution film increases up to around 12 in the entire area; near the front end tip of the galvanized coating beneath the coating film, pH is lowest at about 5. This is because that, similarly to the case in Fig. 6, OH^- continues to increase on the Fe surface thanks to the cathodic protection; however, as the galvanized coating had retrograded by 500 μm , Zn^{2+} is consumed beneath the coating film, and does not reach the solution film on the cut edge surface.

In the case of MgCl_2 500ppm solution shown in Fig. 9(a), Mg^{2+} which used to be contained in the solution becomes $\text{Mg}(\text{OH})_2$ and consumes OH^- , and therefore, the increase of pH is suppressed. Ac-



Fig. 8 Results of numerical analysis under paint film near shear cut edge of galvanized steel sheet in NaCl 500ppm solution⁹⁾

cordingly, Zn^{2+} that eluted from the galvanized coating front end tip beneath the coating film is not fully consumed, reaches the solution film on the cut edge surface, and generates corrosion products afterward. Once Zn^{2+} reaches the cut edge surface, as pH in the vicinity of the exit beneath the coating film decreases, $Mg(OH)_2$ that precipitated in this vicinity re-resolves, and corrosion products of the Zn system are generated instead. Furthermore, as Mg^{2+} migrates to the Fe side with the sacrificial corrosion current, Mg^{2+} of high concentration is generated apart from the galvanized coating part.

In either solution, as shown in Figs. 8(b), (d) and Figs. 9(b), (d), high concentrations of Cl^- and Zn^{2+} are confirmed near the front end tip of the galvanized coating beneath the coating film. As compared with the concentration on the cut edge surface under the same condition shown in Fig. 6, Zn^{2+} concentration becomes higher by about 10 times and the concentration of Cl^- becomes higher by about 20 times.

Figure 8(b) and Fig. 9(b) show that as the anode is aggregated to the front end tip of the galvanized coating and Cl^- is enriched at the position, while the cathode is dispersed all over the Fe surface, Na^+ is not enriched locally anyway. In the case of NaCl solution, as shown in Fig. 8(e)–(g), corrosion products are generated beneath the coating film in a great quantity. In $MgCl_2$ solution, as shown in Fig. 9(e)–(h), corrosion products are generated on the Fe surface of

the cut edge surface in addition to beneath the coating film.

In the NaCl solution, corrosion products aggregate to beneath the coating film, and the type of corrosion products changes in the direction from the front end tip to the cut edge surface. The transitions of pCl and pH on the path from point A to point B at the cut edge end shown in Fig. 8(a) are graphically shown in the equilibrium diagram of pCl and pH⁽¹⁾ in Fig. 10. Figure 10 shows that, in the case that the galvanized coating does not retrograde, as the Zn^{2+} concentration is about 1–10 mol/m³ as shown in Fig. 6 in NaCl 500ppm solution, $ZnCl_2/4Zn(OH)_2$ is not generated and $ZnCl_2/6Zn(OH)_2$ is generated instead. However, when the galvanized coating retrogrades, Zn^{2+} concentration becomes high and Cl^- is enriched at the front end tip of the galvanized coating, and $ZnCl_2/4Zn(OH)_2$ is generated. Thus, even in a solution of low salt concentration of 500 ppm, the concentrations of Zn^{2+} and Cl^- beneath the coating film become 10 times or more higher than those on the cut edge surface, and corrosion products different from those on the cut edge surface are generated.

When the corrosion product distributions in Fig. 8 and in Fig. 9 are compared, in the case of NaCl solution, corrosion products are not generated at all on the Fe surface of the cut edge surface. In the case of $MgCl_2$ solution, even in the geometry where the galvanized coating retrogrades by 500 μ m, corrosion products of the Zn system

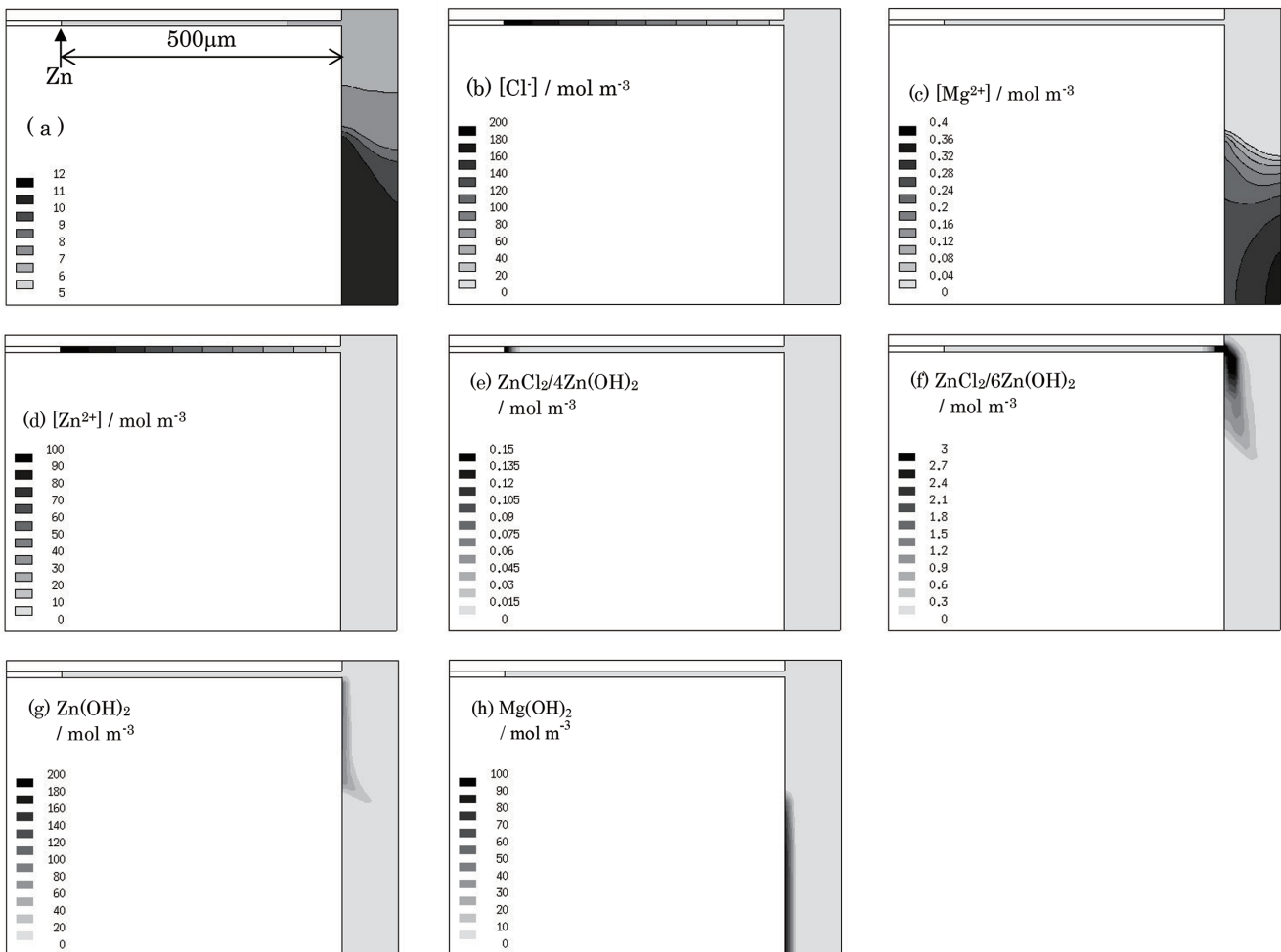


Fig. 9 Results of numerical analysis under paint film near shear cut edge of galvanized steel sheet in $MgCl_2$ 500 ppm solution⁹⁾

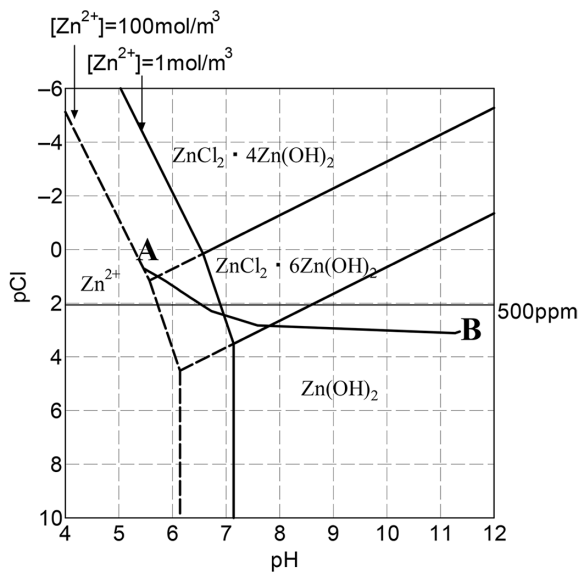


Fig. 10 pCl-pH diagram and a transition of pCl and pH from position A to B in Fig. 8⁹⁾

and $Mg(OH)_2$ are generated on the Fe surface of the cut edge surface. Therefore, when the galvanized coating retrogrades by $500\mu m$ in NaCl solution, although the barrier effect of the corrosion product on the cut edge surface is not obtained, in the solution containing Mg^{2+} , even when the galvanized coating retrogrades to a certain extent, corrosion products are generated on the cut edge surface, and the corrosion resistance thanks to the barrier effect is considered to be obtained.

4. Conclusion

We developed a numerical analysis model for the corrosion phenomena, and verified that the early stage corrosion product distribution in the galvanic corrosion of the Fe/Zn system agrees well with the experimental results. As the result of a study on the corrosion process on the cut edge surface of a galvanized steel sheet by using the model, the following findings were obtained.

- 1) In the case of $MgCl_2$ solution, as the increase of pH on the Fe surface is suppressed by the generation of $Mg(OH)_2$, corrosion products tend to be generated in the neighborhood of the metal surface. In the case of NaCl solution, as pH on the Fe surface

increases as a whole, corrosion products are also generated in the solution apart from the metal surface.

- 2) $Mg(OH)_2$ re-resolves as pH lowers, and corrosion products of the Zn system are generated instead. Accordingly, in the case of $MgCl_2$ solution, as a reason for the higher corrosion resistance than that in NaCl solution, the barrier effect of the corrosion products generated on the Fe surface is considered.
- 3) As the galvanized coating retrogrades from the cut edge surface, and the corrosion beneath the coating film progresses, Zn^{2+} and Cl^- beneath the coating film are enriched and the concentrations become enriched more than 10 times that of those at the cut edge surface. For this, $ZnCl_2/4Zn(OH)_2$ is generated beneath the coating film.

References

- 1) Doig, P., Flewitt, P.E.J.: J. Electrochem. Soc. 126, 2057 (1979)
- 2) Strommen, R.: Corrosion'80. Paper No. 241, 1980
- 3) Warne, M.A.: Corrosion'85. Paper No. 313, 1985
- 4) Morris, R., Smyrl, W.: J. Electrochem. Soc. 136, 3229 (1989)
- 5) Munn, R.S., Devereux, O.F.: Corrosion. 47, 612 (1991)
- 6) Munn, R.S., Devereux, O.F.: Corrosion. 47, 618 (1991)
- 7) Aoki, S., Amaya, K., Miyasaka, M.: Boundary Element Analysis on Corrosion Problems. Tokyo, Shoka-bo, 1998
- 8) Okada, N., Matsumoto, M., Nishihara, K., Kimoto, M., Kudo, T., Fujimoto, S.: Tetsu-to-Hagané. 95, 144 (2009)
- 9) Okada, N., Matsumoto, M., Nishihara, K., Kimoto, M., Kudo, T., Fujimoto, S.: Tetsu-to-Hagané. 97, 108 (2011)
- 10) Okada, N., Matsumoto, M., Nishihara, K., Kimoto, M., Kudo, T., Fujimoto, S.: Zairyo-to-Kankyo. 60, 333 (2011)
- 11) Press, W.H., Teukolsky, S.A., Vetterling, W.T., Flannery, B.P.: Numerical Recipes in C. Tokyo, Gijyutu-Hyoron-sha, 1993, p. 264
- 12) Edited by The Chemical Society of Japan: Chemistry Guide Basic Volume Fifth Revised Edition. Tokyo, Maruzen, 2004, II-562
- 13) Newman, J., Thomas-Alyea, K.E.: Electrochemical System Third Edition. New Jersey, John Wiley & Sons, Inc., 2004, p. 284
- 14) Tamura, H.: Tetsu-to-Hagané. 91, 22 (2005)
- 15) Feitknecht, W.: Chemistry and Industry. 36, 1102 (1959)
- 16) Pauling, L.: General Chemistry. New York, Dover, 1988, p. 456
- 17) Edited by The Electrochemical Society of Japan: New Edition Electrochemical Guide Book. Tokyo, Maruzen, 1964, p. 120
- 18) Lang, W., Zander, R.: Ind. Eng. Chem. Fundam. 25, 775 (1986)
- 19) Matsumoto, M., Okada, N., Nishihara, K., Kimoto, M., Kudo, T.: ISIJ Int. 49, 574 (2009)
- 20) Okada, N., Matsumoto, M., Kimoto, M., Kudo, T.: Proceedings of GALVATECH'07 7th International Conference on Zinc and Zinc Alloy Coated Steel Sheet. Tokyo, ISIJ, 2007, p. 624
- 21) Hayashi, K., Tsujikawa, S.: Zairyo-to-Kankyo. 50, 292 (2001)



Nobuhiro OKADA
Senior Researcher, Doctor of Engineering
Mathematical Science & Technology Research Lab.
Advanced Technology Research Laboratories
20-1 Shintomi, Futtsu City, Chiba Pref. 293-8511



Masamitsu MATSUMOTO
Senior Researcher, Doctor of Engineering
Surface Treatment Research Lab.
Steel Research Laboratories



Katsuhiko NISHIHARA
Senior Researcher, Doctor of Engineering
Materials Characterization Research Lab.
Advanced Technology Research Laboratories